17. The concentration of NO_2 is estimated from the photochemical steady-state relation involving the reaction with O_3 and photolysis as

$$[NO_2] = [NO]\frac{k_{NO\text{-}O_3}[O_3]}{J_{NO_2}} \quad (3)$$

where brackets denote concentration, $k_{NO\text{-}O_3}$ is the reaction rate coefficient of O_3 with NO, and J_{NO_2} is the photolysis rate coefficient of NO_2 to NO (*11*). This assumption can be made because the solar zenith angle is low (55°) and the plume age exceeds a few minutes. The reaction of NO + ClO does not contribute in Eq. 3 because ClO reacts with NO_2 to form $ClONO_2$ within a few minutes in the plume.
18. D. J. Hofmann and J. M. Rosen, *Geophys. Res. Lett.* **5**, 511 (1978).
19. M. R. Williams, in "Proceedings of the Second Conference on the Climatic Impact Assessment Program," *DOT-TSC-OST-73-4*, A. J. Broderick, Ed. (National Technical Information Service, Springfield, VA, 1973).
20. E. A. Brun, *Comité d'Études sur les Conséquences des Vols Stratosphériques (COVOS): Activités 1972–1976* (Société Météorologique de France, Boulogne, 1977).
21. R. C. Miake-Lye *et al.*, *J. Aircr.* **30**, 467 (1991).
22. F. Arnold, J. Scheid, Th. Stilp, H. Schlager, M. E. Reinhardt, *Geophys. Res. Lett.* **19**, 2421 (1992).
23. T. Hanisco *et al.*, in preparation.
24. In the lower stratosphere, the ratio of HO_2 to OH is approximated by

$$\frac{[HO_2]}{[OH]} = \frac{k_{OH\text{-}O_3}[O_3]}{k_{HO_2\text{-}NO}[NO] + k_{HO_2\text{-}O_3}[O_3]} \quad (4)$$

where k_i are associated rate constants (*27*). By Eq. 4, the large decrease in HO_2 in the plume is quantitatively consistent with the large NO values in the plume and O_3 values that are unchanged from background values.
25. J. Zhao and R. P. Turco, *J. Aerosol Sci.*, in press; R. P. Turco *et al.*, *J. Appl. Meteorol.* **19**, 78 (1980); R. C. Miake-Lye, R. C. Brown, M. R. Anderson, C. E. Kolb, paper presented at *Impact of Emissions from Aircraft and Spacecraft upon the Atmosphere*, Deutsche Forschungsanstalt für Luft-und Raumfahrt, Köln, Germany, 18 to 20 April 1994.
26. In addition to the CN counter, a particle spectrometer probe aboard the ER-2 measured the concentration of particles between 0.08 and 2 μm in diameter. This instrument showed no response during the plume encounters, indicating that particles detected by the CN counter were smaller than 0.08 μm.
27. P. O. Wennberg *et al.*, *Science* **266**, 398 (1994).
28. F. Gelbard, and J. H. Seinfeld, *J. Colloid. Interface Sci.* **78**, 485 (1980).
29. The aerosol size distribution produced by the Concorde plume coagulation model for a given plume age (Fig. 4) is assumed to instantaneously mix into a volume representing the stratosphere poleward of 20°N and from 12 to 20 km in altitude. The particle number in the box volume is scaled to match particle emissions for the expected HSCT stratospheric fuel usage, 70×10^9 kg year^{-1} (*2*, *8*), and includes a steady-state background aerosol. The steady-state aerosol mass enhancement, from the input of aircraft-emitted sulfur and the 1-year removal time resulting from transport, is 4.4×10^{-11} kg m^{-3}, approximately equal to the nonvolcanic background aerosol mass loading.
30. D. K. Weisenstein, M. K. W. Ko, J. M. Rodriguez, N.-D. Sze, *J. Geophys. Res.* **98**, 23133 (1993).
31. J. C. Wilson *et al.*, *Science* **261**, 1140 (1993).
32. R. J. Salawitch *et al.*, *ibid.*, p. 1146.
33. P. Newman, private communication.
34. K. R. Chan, S. G. Scott, T. P. Bui, S. W. Bowen, J. Day, *J. Geophys. Res.* **94**, 11573 (1989).
35. D. W. Fahey *et al.*, *ibid.*, p. 11299.
36. R. S. Gao *et al.*, *ibid.* **99**, 20673 (1994).
37. C. R. Webster *et al.*, *Science* **261**, 1130 (1993).
38. K. K. Kelly *et al.*, *J. Geophys. Res.* **94**, 11317 (1989).
39. J. C. Wilson, J. H. Hyun, E. D. Blackshear, *ibid.* **88**, 6781 (1983).
40. M. Loewenstein, J. R. Podolske, K. R. Chan, S. E. Strahan, *ibid.* **94**, 11589 (1989).
41. M. H. Proffitt *et al.*, *ibid.*, p. 16547.
42. Experiments using the Concorde engine were performed in a British high-altitude test cell at the National Gas Turbine Establishment in Pyestock, England, for the following conditions: Mach 1.95, 15.4 to 16.5 km, 227 K, stratospheric water vapor equivalent, and fuel flow of 1.5 kg s^{-1}. These results and theoretical calculations are part of the U.S. Climatic Impact Assessment Program (CIAP) (*10*).
43. Experiments were conducted on the Olympus 593 Mk 602 (production version) engine in a high-altitude test cell at the French Centre d'Essais des Propulseurs de Saclay of the Société Nationale d'Étude et de Construction de Moteurs d'Aviation for the following conditions: Mach 2.0, 16.2 km, 222 K, stratospheric water vapor equivalent, and fuel flow of 1.6 kg s^{-1}. These results are part of COVOS (*20*).

44. We appreciate the efforts of pilots J. Barrilleaux of NASA and F. Rude of Air France in acquiring this data set; Aerospace Fuels Laboratory of the U.S. Air Force in analyzing the fuel samples; J. A. Eilers, M. Craig, R. M. Stimpfle, and M. H. Proffitt for ClO and O_3 data; D. K. Weisenstein and B. Massé for helpful discussions; and many others in France and New Zealand for ground support operations. K.A.B. acknowledges the support of a Global Change Distinguished Postdoctoral Fellowship from the U.S. Department of Energy. The High-Speed Research and Upper Atmosphere Research programs of NASA have supported this research.

28 April 1995; accepted 26 July 1995

P′P′ Precursors Under Africa: Evidence for Mid-Mantle Reflectors

Yves Le Stunff,* Charles W. Wicks Jr.,† Barbara Romanowicz

Observations of precursors to P′P′ from a recent exceptionally large deep earthquake in the Fiji Islands (moment magnitude = 7.6) at an array of broadband stations in California revealed mid-mantle reflectors near depths of 785 kilometers and 1200 kilometers under the southern African rift. Such observations, previously reported primarily in subduction zones, suggest that these reflectors may have a global character. Our analysis, which also indicated a sharp, uplifted 670-kilometer discontinuity, demonstrates the power of sparse regional broadband arrays for the study of weak, frequency-dependent features in deep-Earth structure.

Several studies around 1970 suggested the existence of steep velocity gradients or discontinuities at various depths in the Earth's mantle (830 km, 900 km, and 1200 km) and in various regions (*1*–*3*), but reference global Earth models developed since the 1970s have not found a compelling need for any of them. More recently, contrasts in seismic velocity or impedance have been identified near subduction zones at depths of 900 km (*4*–*6*) and 1200 km (*6*). The observation of precursors to PKPPKP (P′P′) has allowed investigation of mantle discontinuities of regions like Antarctica and the mid–Indian Ocean ridge with some success (*2*, *7*, *8*), but so far continents have been poorly sampled. The array-processing techniques appear to be the best for the detection of these phases (*9*–*11*); they enable us to suppress ambient noise and properly estimate the slowness of the seismic phases.

On 9 March 1994, a deep earthquake occurred in the Fiji islands [latitude, −18.039; longitude, −178.413; depth, 563 km; origin time, 23:28:06.7; moment magnitude (M_ω), 7.6], the largest in this region since the deployment of new generation broadband stations worldwide. This event was recorded on 22 broadband stations in California (Fig. 1A). The location of the surface bounce points of P′P′ follows a northeast-southwest trend south of Lake Tanganyika in a region where the African Rift is bending in a southeastern direction toward the Lake Malawi region (Fig. 1B). We now demonstrate the potential of the sparse broadband network to detect and characterize, in a wide frequency band, weak phases such as precursors to P′P′ and identify discontinuities in the mantle. We use observations of the same event on the dense California short-period arrays (Fig. 1A) [Northern California Seismic Network (NCSN) and Southern California Seismic Network (SCSN)] to check the validity of the broadband observations in the common frequency band (0.2 to 5 Hz).

P′P′ precursors have previously been observed at epicentral distances of ~70° for which P′P′ usually has high amplitude given the temporal proximity of arrivals of different core branches. Our stations lie in a range from 76.4° to about 80.2° where only the DF branch (which travels through the inner core) is expected to be seen. As our ray tracing experiments demonstrate (Fig. 2), this is an ideal distance range to look for mantle discontinuities at depths of 650 to 1100 km.

We stack the broadband (BB) and the short period (SP) arrays using three different bandpass filters: 3.5 to 12 s, 2.5 to 4 s, and 1.5 to 3 s (Fig. 3). In the bandpass 3.5 to 12 s for the BB stack (Fig. 3A), there are

Seismographic Station and Department of Geology and Geophysics, University of California at Berkeley, Berkeley, CA 94720, USA.

*To whom correspondence should be addressed.
†Present address: Institut für Geophysik, D-37075 Göttingen, Germany.

two main energy arrivals, at about 245 s and 180 s before P'P'. We have tried to explain these phases in terms of standard phases (like PcPPKP or SKKP), but none of our ray-tracing experiments was successful in matching slowness or arrival time. P'P' precursors reflected at a depth of about 1180 km and 785 km match the arrival times as well as the observed differential slownesses (1.3 s per degree for the first arrival, mainly BC branch, and 2.0 s per degree for the second one, mainly AB and BC branches) (Fig. 2B). In the SP stack for the same frequency band (Fig. 3D), one single phase is clear and common to both stackings: the P'785P' phase. A comparison of spectral amplitudes of linear stacks shows (Fig. 4) that no signal is recorded on the SP instruments above 5 s, providing a possible explanation why the 1180-km reflection cannot be seen on the SP stack. At slightly higher frequency (Fig. 3B), the main phase appears about 149 s before the main P'P' arrival. The differential slowness suggests that this arrival corresponds to the DF branch of a precursor reflected at a depth of 655 km. For this depth, this is the main expected phase (Fig. 2B). In this frequency range, there is again energy arriving about 180 s before the main phase (P'785P') with a slowness comparable to that at lower frequency (Fig. 3A). Little energy is seen at

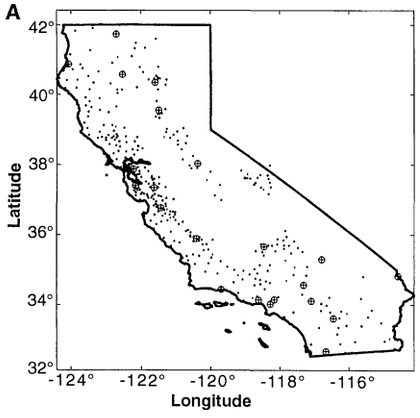

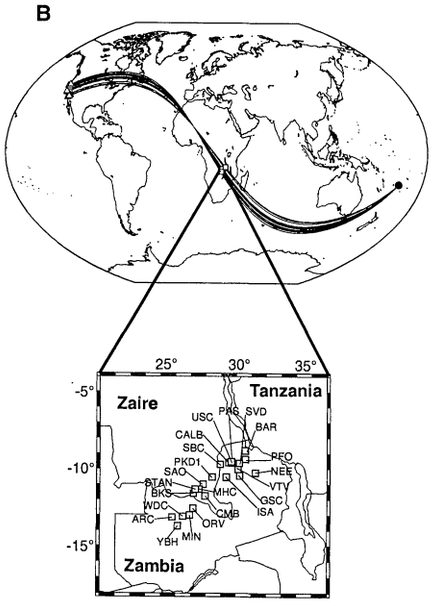

Fig. 1. (**A**) Geographical distribution of recording stations. Circles are BB stations (11 Berkeley Digital Seismic Network and 11 TERRAscope stations). Dots are 342 SP stations of the SCSN and NCSN. The SP arrays have previously been used for P'P' precursor studies (*13*). (**B**) Source-receiver geometry. The enlarged plot shows surface bounce points near the southeastern extension of the African Rift. Corresponding names of BB stations in California are indicated.

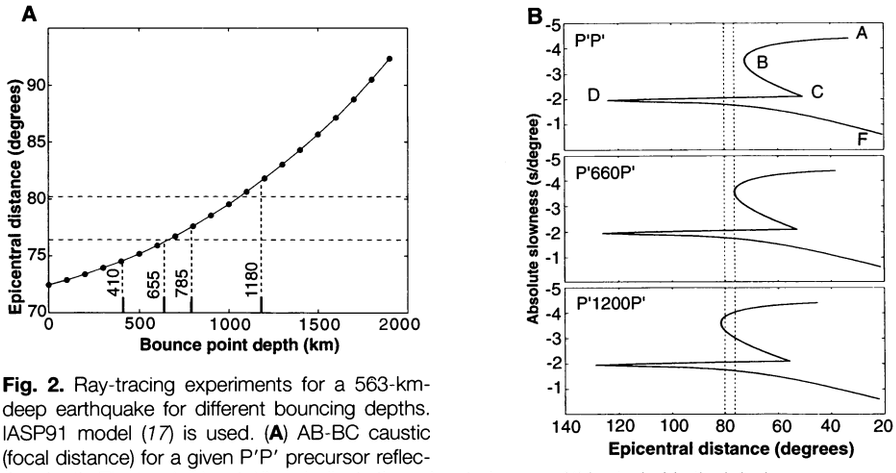

Fig. 2. Ray-tracing experiments for a 563-km-deep earthquake for different bouncing depths. IASP91 model (*17*) is used. (**A**) AB-BC caustic (focal distance) for a given P'P' precursor reflection depth. The two horizontal lines indicate the epicentral range of this study. Vertical dashes correspond to mantle discontinuities. The caustic area is reached for P'P' precursors bouncing between 670 and 1070 km; even if the reflection coefficient is small, precursors may be observable for deep discontinuities. (**B**) Slowness (s/degree) as a function of epicentral distance (degrees) for three different bounce point depths. Names of different branches are marked on the top panels of each plot. Vertical lines indicate the distance range of our observations. Discontinuities above 600 km (like the 400-km discontinuity) would be difficult to observe unless their reflection coefficients are particularly high.

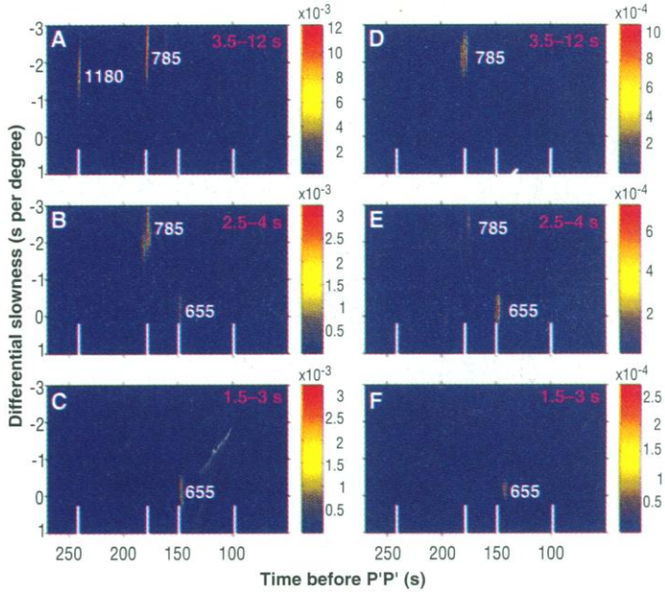

Fig. 3. Stacking results for a time window from 270 to 50 s before P'P', using a nonlinear 3rd-root stacking method (*35*). BB stacks are on the left (A to C) and SP stacks are on the right (D to F). The square of amplitude is plotted as a function of time (s) and slowness (s/degree) relative to the arrival of P'P' across the array. Vertical color bars indicate the ratio of the maximum precursor stacked amplitude to maximum P'P' stacked amplitude. Data are bandpass-filtered between 3.5 to 12 s (**A** and **D**), 2.5 to 4 s (**B** and **E**), and 1.5 to 3 s (**C** and **F**). All traces are first aligned and normalized with respect to the P'P' phase. Bars on the *x* axis indicate theoretical arrival times for precusors (from left to right: 1180 km, 785 km, 655 km, and 400 km). The stacks are exceptionally clean in the interval between 400 and 50 s before P'P'. The ratio obtained through stacking 342 SP stations is about one-third lower than with the BB stations (*36*), which is not the case with linear stacking. No energy arrival is seen near the theoretical arrival corresponding to a reflector of ~670 km, in either stack, for the low-frequency window (A and D). No significant energy is observed in any of the frequency bands from a discontinuity near 400 km, in agreement with what is predicted from Fig. 2. This absence may be also explained by topography on this discontinuity (*11*).

~245 s before P'P', indicating a frequency dependence of the phase P'1180P' observed in Fig. 3A. The SP stack (Fig. 3E) is comparable to the BB stack.

In the period range 1.5 to 3 s (Fig. 3, C and F), the P'655P' arrival, 149 s before P'P', is the dominant phase. This observation confirms that this event is particularly energetic and that the source-array geometry is highly favorable. Little energy is seen at ~245 s and 180 s.

The frequency dependence of the observed energy arrivals may indicate that the corresponding mid-mantle reflectors have some topography or variations in thickness (*11*). To investigate this further, we grouped our stations in different clusters and looked in the highest frequency range (1.5 to 3 s) for possible energy arrivals at ~250 s. We found a regional clustering following a roughly north-south trend (Fig. 5) with consistent, clear energy arrivals. The most characteristic feature is a variation, for BB and SP stacks, in arrival times with clustering for the 1180-km reflected phases (up to 6 s between cluster 1 and cluster 3), implying a variation of the reflector depth (of 30 km). This variation is not observed for the 655-precursor and is therefore difficult to explain in terms of varying near-station or surface bounce-point effects. The 785-precursor is not observed at this frequency. The energy arrivals have a slowness that differs by 1.3 s per degree from the observation at lower frequency, where another branch (BC) was observed (Fig. 2B). We estimate that a dip of 4° to 6° on the interface (to northwest, that is, in the direction of the azimuthal plane) could result in this shift in apparent differential slowness (the BC branch being reflected as a DF branch at the interface). This dip corresponds to 30 km of topographic variation in a distance of 400 km, essentially the same variation inferred from the travel-time differences shown in Fig. 5.

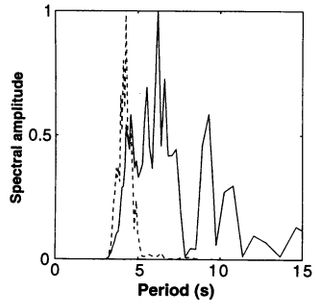

Fig. 4. Amplitude spectra for SP (dashed line) and BB (solid line) linear stacks bandpassed between 3.5 and 12 s (compare Fig. 3, A and D). No energy is detected by SP instruments above 5 s, whereas the BB signal has a broader frequency content. This may explain the absence of the P'1180P' phase in the SP stacks. The spectra of these instruments are comparable in the other frequency windows of Fig. 3.

The BB complete stacks show an unexpected observation of the 670-km discontinuity. It is observed in the range 1.5 to 3 s, implying a sharp discontinuity [less than 5 km (*12*)] in agreement with other SP observations (*10, 13*). The fact that energy is not observed in the lowest frequency range implies a more complicated zone, in which a sharp discontinuity might be associated with a high-velocity gradient zone (*14–16*) (creating low-frequency destructive interference) or where large-scale topography implies defocusing of the waves (*11*). The clustering experiment suggests, however, no significant local topography. The estimated depth (655 km) is obtained with the radially symmetric IASP91 model (*17*). However, lower than average velocities in the uppermost mantle may exist under south central Africa, as indicated by arguments in favor of a rift continuation in this region, on the basis of seismicity (*18, 19*) and heatflow measurements (*20*). Recent tomography models also display a slower than average mantle in the topmost 300 km in this area (*21*). Therefore, an actual depth as shallow as 650 to 645 km is not excluded, in agreement with results by Shearer and Masters (*22*), although these authors had poor resolution in this region. Given the negative Clapeyron slope of the 670-km discontinuity (*23*), this result would imply a hotter than average mantle in the region of our bounce points.

It is unlikely that the energy arrivals, interpreted as P'785P' and P'1180P', would be due to scatterers near the core mantle boundary, given their early arrival times in front of the main P'P' phase and the size of the array (*24*). The frequency dependence of the 785-km reflector suggests that the reflector is rather sharp and has a maximum thickness of 7 to 10 km. The nature of this reflector is not clear. It could be related to observations in the same depth range in other regions, such as in the northeastern Pacific, near 830 km (*1*). More recently, Petersen *et al.* (5) have observed S-wave impedance contrasts and Kawakatsu and Niu (*4*) have observed S-wave velocity contrasts at depths of ~900 km in subduction zones. Relatively large depth differences (~50 km) are apparent in adjacent areas (*4*, 6), implying significant topography. The region of study could be the site of hot upwellings, possibly related to the "great south African plume" (*25*), seen as a broad zone of very low velocities in the lowermost mantle in recent tomographic models (*26–28*). The uplifted "900 km discontinuity" described here would then indicate a strongly negative Clapeyron slope, if it is a phase change (*29*).

The deepest reflector seems rather complicated. Low-frequency observations imply a maximum thickness of 20 to 25 km. The fact that, at higher frequencies, this reflector is seen on subarrays but not on complete stacks, is an indication of a complex structure with some sharp features. It is possible that the absence of high frequencies on the complete stacks is due to defocusing of energy caused by a dipping interface or that we are looking at a zone of random reflectors or scatterers. The similarity of the depth range of these reflectors with obser-

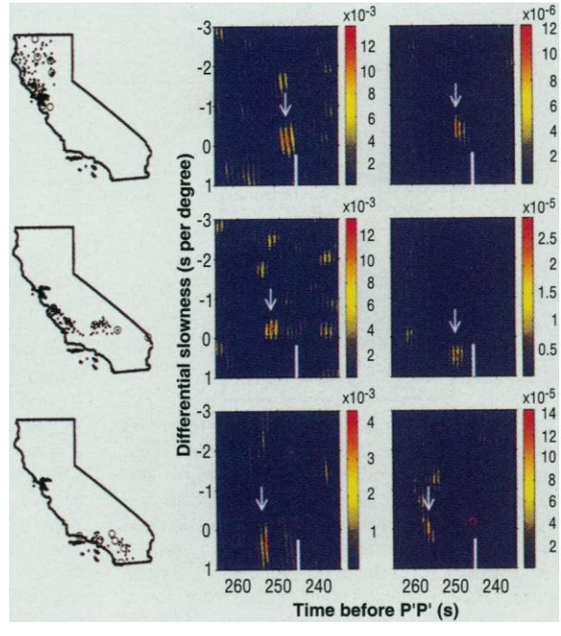

Fig. 5. Regional stacks for three clusters of stations, in the highest frequency range of Fig. 3 (1.5 to 3 s) for time windows from 265 to 235 s. The first column shows the different clusters, the second and third columns, the corresponding BB and SP stacks, respectively. Although the stacks are noisier than in Fig. 3 for the BB stations (because fewer stations are used in each of them), they do show consistent main arrivals between 300 and 50 s before the P'P' arrival. Vertical bars indicate theoretical arrival times for precursors. Arrows indicate arrivals identified as corresponding to P'1180P'. The amplitude varies as a function of the number of stations because of the nonlinearity of the stack. This is seen when comparing BB and SP stacks, but also SP stacks for C1 and C3 where 1108 and 35 stations, respectively, are used. BB and SP stacks are similar. No time variation is observed for the 655-precursor. The 785-precursor is not consistently seen.

vations of a discontinuity near 1150 km in subduction areas [(3, 6), for example] indicates that this may be a global feature of yet unknown nature.

The observation of reflectors at mid-mantle depths comparable to those in subduction zones, but in a different environment, indicates that a search for yet unidentified mineral assemblages of global significance may be worthwhile. Recent experiments have shown the possible existence of phase transitions at lower mantle conditions: orthorhombic-to-cubic silicate perovskite (30) and rutile SiO_2 to $CaCl_2$ structure (31). The role and proportions of volatiles such as water or carbon dioxide in the mantle remain largely unknown and could be of importance (32).

Additional seismic observations with the great resolving power of BB arrays should help answer the question of the global character of our observations.

REFERENCES AND NOTES

1. L. R. Johnson, *Bull. Seismol. Soc. Am.* **59**, 973 (1969).
2. J. H. Whitcomb and D. L. Anderson, *J. Geophys. Res.* **75**, 5713 (1970).
3. L. P. Vinnik, A. A. Lukk, A. V. Nikolaev, *Phys. Earth Planet. Inter.* **5**, 328 (1972).
4. H. Kawakatsu and F. Niu, *Nature* **371**, 301 (1994).
5. N. Petersen, J. Gossler, R. Kind, K. Stammler, L. Vinnik, *Geophys. Res. Lett.* **20**, 281 (1993).
6. C. W. Wicks and M. A. Richards, *Eos Fall Suppl.* **74**, 550 (1993).
7. E. R. Engdahl and E. A. Flinn, *Science* **163**, 177 (1969).
8. R. D. Adams, *Bull. Seismol. Soc. Am.* **61**, 1441 (1971).
9. I. Nakanishi, *Geophys. Res. Lett.* **13**, 1458 (1986).
10. _____, *Geophys. J. Int.* **93**, 335 (1988).
11. J. P. Davis, R. Kind, I. S. Sacks, *ibid.* **99**, 595 (1989).
12. P. G. Richards, *Z. Geophys.* **38**, 517 (1972).
13. H. M. Benz and J. E. Vidale, *Nature* **365**, 147 (1993).
14. L. P. Vinnik, R. A. Avetisjan, N. G. Mikhailova, *Phys. Earth Planet. Int.* **33**, 149 (1983).
15. N. Petersen *et al.*, *Geophys. Res. Lett.* **20**, 859 (1993).
16. V. S. Solomatov and D. J. Stevenson, *Earth Planet. Sci. Lett.* **125**, 267 (1994).
17. B. L. N. Kennett and E. R. Engdahl, *Geophys. J. Int.* **105**, 429 (1991).
18. C. H. Scholz, T. A. Koczynski, D. G. Hutchins, *Geophys. J. R. Astron. Soc.* **44**, 135 (1976).
19. G. S. Wagner and C. A. Langston, *Geophys. J. Int.* **94**, 503 (1988).
20. D. S. Chapman and H. N. Pollack, *Tectonophysics* **41**, 79 (1977).
21. S. P. Grand, *IUGG Abstr. Week B* **74**, 395 (1995).
22. P. M. Shearer and T. G. Masters, *Nature* **355**, 791 (1992).
23. E. Ito and E. Takahashi, *J. Geophys. Res.* **94**, 10637 (1989).
24. R. A. W. Haddon, E. S. Husebye, D. W. King, *Phys. Earth Planet. Int.* **14**, 41 (1977).
25. A. M. Dziewonski, A. M. Forte, W.-J. Su, R. L. Woodward, *AGU Geophys. Monogr.* **76**, 67 (1993).
26. W.-J. Su, R. Woodward, A. M. Dziewonski, *J. Geophys. Res.* **99**, 6945 (1994).
27. T. G. Masters, H. Bolton, P. Shearer, *EOS Spring Suppl.* **73**, 201 (1992).
28. X. D. Li and B. Romanowicz, *Geophys. J. Int.* **121**, 695 (1995).
29. Bukowinski and Wolf (33) calculate that changes in symmetry of silicate perovskite would involve a positive Clapeyron slope. If the 900-km discontinuity has a negative slope as we suggest, this would rule out a structural change in perovskite as a cause of the 900-km discontinuity, in agreement with (34).
30. C. Meade, H. K. Mao, J. Hu, *Science* **268**, 1743 (1995).
31. K. J. Kingma, R. E. Cohen, R. J. Hemley, H.-K. Mao, *Nature* **374**, 243 (1995).
32. J. A. Tyburczy, T. S. Duffy, T. J. Ahrens, M. A. Lange, *J. Geophys. Res.* **96**, 18011 (1991).
33. M. S. T. Bukowinski and G. H. Wolf, *ibid.* **95**, 12583 (1990).
34. L. Stixrude and R. E Cohen, *Nature* **364**, 613 (1993).
35. K. J. Muirhead and R. Datt, *Geophys. J. R. Astron. Soc.* **47**, 197 (1976).
36. This amplitude difference comes from the fact that there is less coherence in the SP data than in BB data, so that using a large number of stations attenuates small signals, whereas larger signals are unaffected. This is, however, concomitant to a reduction in noise amplitude (35) so that coherent phases can be detected.

37. We thank L. Vinnik for comments and suggestions and J. Vidale for providing short-period array data. This study was partially supported by the France-Berkeley Fund and is the Berkeley Seismographic Station contribution 95-6.

1 May 1995; accepted 1 August 1995

Coherent Laser Control of the Product Distribution Obtained in the Photoexcitation of HI

Langchi Zhu, Valeria Kleiman, Xiaonong Li, Shao Ping Lu,* Karen Trentelman,† Robert J. Gordon‡

Active control of the distribution of products of a chemical reaction was demonstrated by using a method based on the principle of quantum mechanical interference. Hydrogen iodide (HI) molecules were simultaneously excited above their ionization threshold by two competing pathways. These paths were absorption of three ultraviolet photons of frequency ω_1 and one vacuum ultraviolet photon of frequency $\omega_3 = 3\omega_1$. The HI^+ and I^+ signals were modulated as the phase between the lasers was varied, with the HI^+ signal lagging by 150° ± 15°. A mechanism consisting of autoionization and predissociation is proposed.

A fundamental goal in synthetic chemistry is to develop methods for maximizing the yield of a desired compound while reducing the yields of unwanted by-products. The traditional approach to this problem is to modify the experimental conditions (such as temperature, pressure, or pH) so as to optimize the product distribution. This is a passive strategy in that it relies on the natural response of the chemical system to external conditions, and there is no guarantee that there exist conditions that could produce the desired result. For example, one may wish to photodissociate the stronger of two bonds in a molecule. Although for some molecules it may be possible to find wavelengths of light that can accomplish this task (1), for many others the weakest bond breaks preferentially at any wavelength.

In recent years, a number of strategies have been proposed to achieve more active control of chemical reactions (2). The central idea is to manipulate the reacting molecule with electromagnetic fields, which allow the experimenter to guide the molecule along the desired reaction path. We report here active experimental control of the distribution of products in a chemical reaction.

One approach for controlling chemical reactions, developed by Tannor, Rice, and co-workers (3), is to excite a molecule with a sequence of ultrashort light pulses. This method has been used, for example, by Gerber and co-workers (4) to control the ionization and fragmentation of Na_2.

Another approach to active control is based on the principle of quantum-mechanical interference. This principle states that if there exist more than one independent way of reaching a final state, the overall probability of reaching that state includes the probabilities of the individual paths and contributions arising from interference between them. The best known example of this principle is the interference of particles passing through a pair of slits before hitting a screen. The intensity of particles reaching some point on the screen is the sum of the intensities obtained from each slit independently, plus an interference term that depends on the relative distance of the point from the two slits.

The photochemical analog of the two slit experiment was first proposed by Brumer and Shapiro (3). Their strategy involves the simultaneous excitation of a molecule by two different pathways connecting the same initial and final states. The probability for each independent transition is given by:

$$P_n \propto |\langle \Psi_f | \hat{O}_n | \Psi_i \rangle|^2 \qquad (1)$$

where ψ_i and ψ_f are the time-independent

Department of Chemistry (m/c 111), University of Illinois at Chicago, Chicago, IL 60607–7061, USA.

*Present address: Department of Chemistry, Indiana University, Bloomington, IN 47405, USA.
†Present address: Detroit Institute of Arts, 5200 Woodward Avenue, Detroit, MI 48202, USA.
‡To whom correspondence should be addressed.